energies

MDPI

Article

A Novel Phase Current Reconstruction Method for a Three-Level Neutral Point Clamped Inverter (NPCI) with a Neutral Shunt Resistor

Yungdeug Son [1] and Jangmok Kim [2,*]

[1] Department of Mechanical Facility Control Engineering, Korea University of Technology and Education; Cheonan, Chungnam 31253, Korea; ydson@koreatech.ac.kr
[2] Department of Electrical and Computer Engineering, Pusan National University, Busan 46241, Korea
* Correspondence: jmok@pusan.ac.kr; Tel.: +82-51-510-2366

Received: 1 September 2018; Accepted: 25 September 2018; Published: 1 October 2018

Abstract: This paper presents three phase current reconstruction methods for a three-level neutral point clamped inverter (NPCI) by measuring the voltage of a shunt resistor placed in the neutral point of the inverter. In order to accurately acquire the phase currents from the shunt resister, the dwell time of the active voltage vectors need to exceed the minimum time. On the other hand, if the time of active voltage is shorter than the minimum time, the current measurement becomes impossible. In this paper, unmeasurable regions for current are classified into three areas. Area 1 is a region in which both phase currents can be measure. Therefore, it is not necessary to restore the current. In Area 2, only one phase current can be measured. Thus, an estimation or restoration method is needed to measure another phase current. In this paper, the current estimation method using an electrical model of the motor is proposed. Area 3 is the region in which both phase currents can not be measured. In this case, it is necessary to move the voltage vector to the current measurable area by injecting the voltage. In this paper, Area 3 is divided into 36 sectors to inject optimal voltage. The proposed methods have the advantages of high current measurement accuracy and low THD (total harmonic distortion). The effectiveness of the proposed methods are verified through experimental results.

Keywords: alternating current (AC) motor drive; current estimation; current reconstruction method; current unmeasurable areas; total harmonic distortion (THD); single shunt resistor; space vector pulse width modulation (SVPWM); shift method; minimum voltage injection (MVI) method; three-level neutral point clamped inverter (NPCI)

1. Introduction

Two-level inverters are used in most home appliances, such as washing machines, refrigerators, and air conditioners, due to their simple structure, and high reliability and performance. However, in order to overcome the limitations of the efficiency and harmonics of the two-level inverter, three-level inverters have been recently investigated. The three-level neutral point clamped inverter (NPCI) has a structure characteristic of having a neutral point in the direct current (DC) stage, and thus has excellent electro magnetic interference (EMI) and electro magnetic compatibility (EMC) characteristics, due to a low voltage variation rate when switching [1–4]. Unlike a two-level inverter, each arm of a three-level NPCI consists of four switches and two clamping diodes, as shown in Figure 1. When the DC-link voltage is V_{dc}, the voltage of each capacitor is $V_{dc}/2$. The neutral point is connected to each phase output node by the clamp diodes and switches. Due to this structural feature, the three-level NPCI can output either $V_{dc}/2$ or $-V_{dc}/2$ by turning on the two switches located in the upper or lower side of a phase. When the switches of S_{x3} and S_{x4} are turned on, the node voltage of

the x phase is 0 due to the connection with the neutral point through the diodes and switches, where x represents A, B, and C.

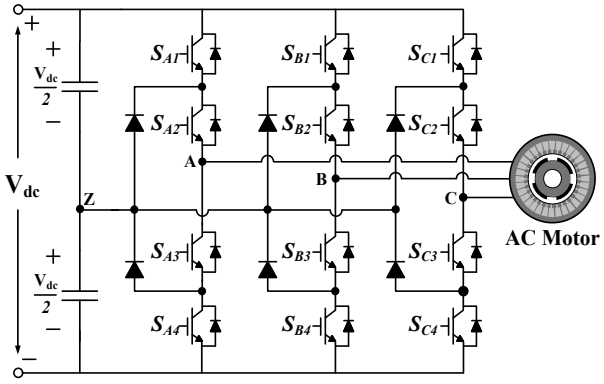

Figure 1. Three-level neutral point clamped (NPC) inverter.

For controlling the AC motor, the controller of the inverter requires the values of the three phase currents, which can be acquired through current sensors or a shunt resistor. A phase current sensing inverter (PCSI), as shown in Figure 2a, is a typical three-phase voltage source inverter with two phase current sensors. It requires at least two current sensors and sensing circuits, which raise the cost of the appliances [5]. For this reason, a DC link shunt resistor R_{shunt} can be used to measure the phase current, as shown in Figure 2b,c. A multi-shunt inverter (MSI) obtains the phase current from the shunt resistor located in the neutral and bottom of the DC link [6]. Measurement of the currents through the shunt resistors is possible when the current flows into the shunt resistor. Since the shunt resistors are located between the neutral and bottom of the DC link, it is possible to measure the phase current only if the active voltage vectors are combined with "O" or "N" switching states. However, although the active vectors are combined with "O" or "N" switching states, the phase current cannot be measured due to the short dwell time of the active vectors. The portion in the space vector diagram where the dwell time of the active vectors is not large enough to measure the current is called the current-unmeasurable area (CUA) [7–24]. A shunt resistor at the neutral point of the three-level NPCI can be used to measure the phase current, as shown in Figure 2c. This is similar to MSI, but a phase current is only obtainable when applying the state of "O" in the switching combination of the effective voltage vector. NPCI is effective in terms of volume and cost as compared to PCSI and MSI. It also has one current sensing circuit, which reduces the ripples caused by current sensor offset and scaling errors [6,7]. However, it has a limited time to sample the phase current in the shunt resistor over one period compared to the PCSI and MSI, so that the unmeasurable areas are widened in the output voltage hexagon. In order to overcome the limitations, some researchers have been interested in NPCI topology for phase current reconstruction.

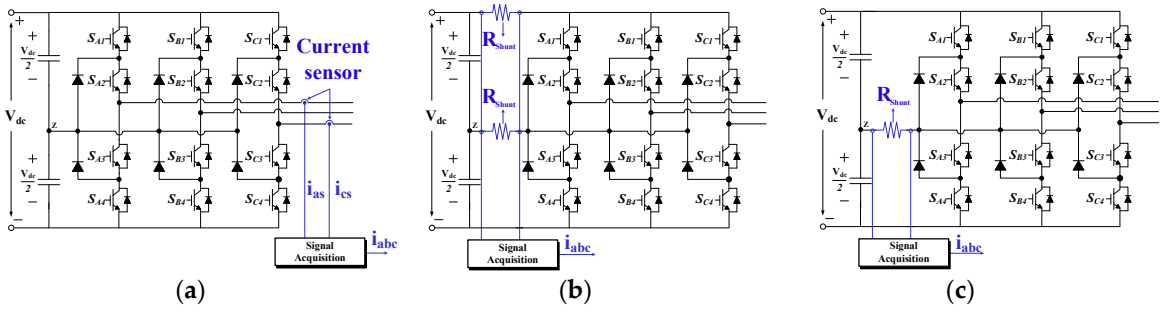

Figure 2. Measurement methods of phase current. (**a**) Conventional phase current sensing inverter (PCSI); (**b**) multi-shunt inverter (MSI); (**c**) neutral point clamped inverter (NPCI).

Previous research has established the effective voltage time by shifting the pulse width modulation (PWM) or injecting the voltage to restore the current [6–24]. However, these methods cause a high total harmonic distortion (THD) by injecting relatively large voltages. In [6], the minimum voltage injection (MVI) method minimizes voltage distortion and operating noise through THD reduction, but this method does not completely reconstruct the phase current at very high modulation index (MI). In addition, the PWM shifting method of [7] also generates harmonics due to asymmetric voltage modulation.

In this paper, the phase current unmeasurable region is classified into three areas, and the current reconstruction methods are proposed according to each area. First, two phase currents can be measured in Area 1, and the normal operation is executed in this area. On the other hand, only 1 phase current can be acquired in Area 2. In this case, the other phase current can be estimated by combining the q-axis current reference obtained from the speed controller and the electrical model of the motor [10]. Lastly, Area 3 is defined as an area where no current can be measured. For measuring the current in this area, the optimal voltage injection method is proposed [12]. To realize this, the hexagon of SVPWM is divided into 36 sectors, and the optimum injection voltage according to the sector is calculated. In addition, the current accuracy and THD are compared with the conventional method [6] in various MI conditions. The proposed method is verified through experimental results.

2. Acquiring Phase Current from Neutral Shunt Resistor

The operation of each three-level NPC inverter phase leg can be represented by a combination of the three switching states "P", "O", and "N". According to these switching states, the inverter has 27 possible combinations of switching states consisting of 24 effective voltage vectors and 3 zero voltage vectors. Because the NPCI has the shunt resistor at the neutral point, the phase current can be acquired only when the effective voltage vector includes the "O" switching state [6]. For example, the A phase current can be measured when the effective vector "O", "N", and "N" is applied to the inverter, as shown in Figure 3.

The 27 switching states of the neutral point clamped (NPC) inverter and the respective measurable phase currents are listed in Table 1. In addition, Figure 4 shows the switching vector in the spatial coordinates of the hexagon. Figure 4 and Table 1 show that the current cannot be measured through the neutral-point shunt resistor during the zero vector (V_0) and space vectors represented by V_1 to V_6.

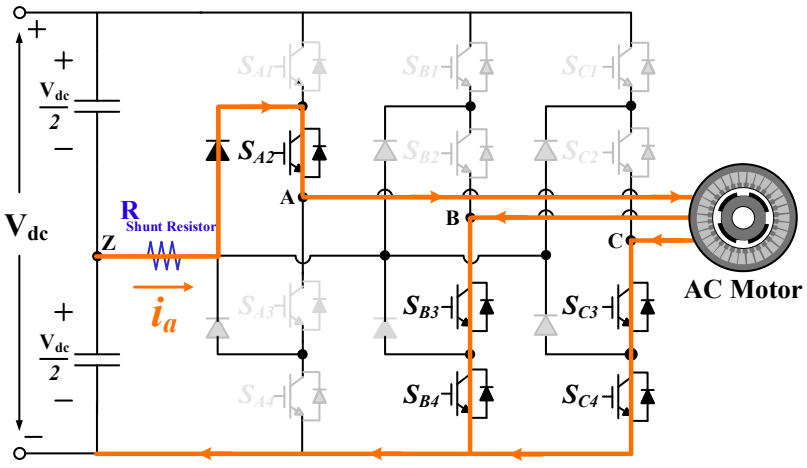

Figure 3. Current path of neutral shunt resistor when effective vector "O", "N", and "N" is applied to the inverter.

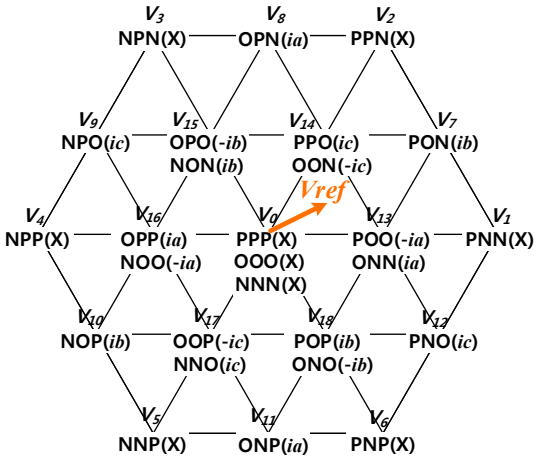

Figure 4. Three-level neutral shunt inverter effective-voltage vector hexagon.

Table 1. Switching states and acquiring the phase current from the shunt resistor.

Space Vector	Switching State		Acquiring Current from the Shunt Resistor		Vector Classification
V_0	[PPP], [OOO], [NNN]		X		Zero vector
	P-type	N-type	P-type	N-type	
V_{13}	[POO]	[ONN]	$-i_a$	i_a	
V_{14}	[PPO]	[OON]	i_c	$-i_c$	
V_{15}	[OPO]	[NON]	$-i_b$	i_b	Effective vector (Small vector)
V_{16}	[OPP]	[NOO]	i_a	$-i_a$	
V_{17}	[OOP]	[NNO]	$-i_c$	i_c	
V_{18}	[POP]	[ONO]	i_b	$-i_b$	
V_7, V_8	[PON], [OPN]		i_b, i_a		Effective vector (Medium vector)
V_9, V_{10}	[NPO], [NOP]		i_c, i_b		
V_{11}, V_{12}	[ONP], [PNO]		i_a, i_c		
V_1, V_2	[PNN], [PPN]		X, X		Effective vector (Large vector)
V_3, V_4	[NPN], [NPP]		X, X		
V_5, V_6	[NNP], [PNP]		X, X		

In one period of the three-level SVPWM, the sampling point and measurable phase current are expressed as shown in Figure 5. In this case, the "a" phase current can be measured in the "ONN" switching state and the "c" phase current can be measured in the "OON" switching state. The other phase current is calculated using Equation (1):

$$i_a + i_b + i_c = 0 \tag{1}$$

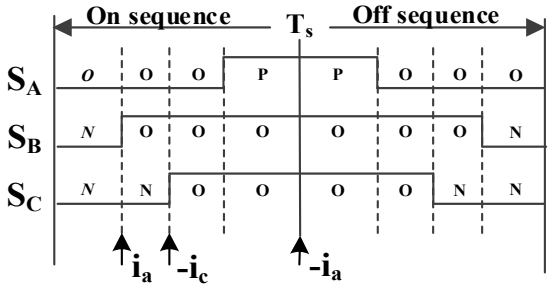

Figure 5. One period of the SVPWM method and sampling point.

3. Current Unmeasurable Areas

The sampling time for measuring the accurate current should have minimum delay from the point of switching time. This is to avoid the current ripple component in the current damping process by switching, as shown in Figure 6a. The minimum time T_{min} is determined using Equation (2) [9]:

$$T_{min} = T_{dead} + T_{settling} + T_{ad} \tag{2}$$

where T_{dead} is the dead time to avoid arm-short of the inverter, $T_{settling}$ is the settling time of the neutral-point current, and T_{ad} is the sample and hold time of the A/D converter. Thus, in order to acquire the phase current properly, the switching time should be greater than T_{min}. Figure 6b shows switching state when the voltage modulation index is changed from Figure 5. In the case of "ONN", since the switching time T_a in the "O" state is larger than T_{min}, accurate "a" phase current can be obtained. However, in the case of "OON", since the switching time T_c of the "O" state is shorter than T_{min}, it is impossible to obtain current on the "c" phase in this state. The areas where the effective voltage dwell time is less than T_{min} are defined as CUAs (current unmeasurable areas). The CUAs in sector 1 of the three level SVPWM hexagon are shown in Figure 7a. In Figure 7a, Area 1 is a region where all phase currents are measurable, Area 2 is a region where only one phase current is measurable, and Area 3 is defined as a current unmeasurable region. The CUAs in all areas of the SVPWM are shown in Figure 7b.

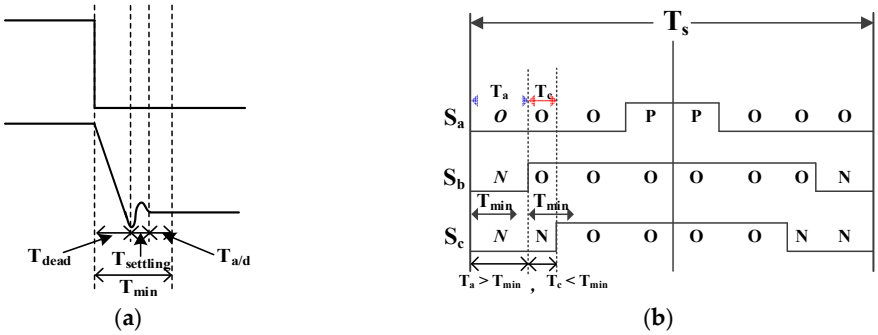

Figure 6. T_{min} and T_s of the SVPWM method. (**a**) Minimum time (T_{min}); (**b**) one PWM period (T_s).

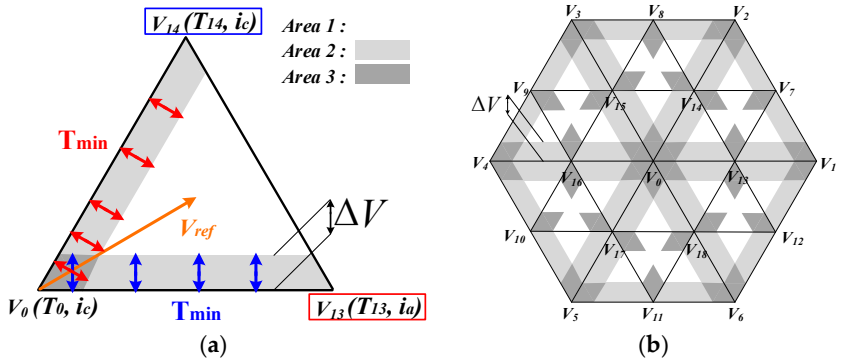

Figure 7. Current-unmeasurable areas (CUAs). (**a**) Sector 1; (**b**) reference-voltage vector hexagon.

In addition, the amplitude of the CUAs ΔV is obtained by Equation (3) [10].

$$T_{min} \ : \ \frac{T_s}{2} = \Delta V \ : \ \frac{V_{dc}}{\sqrt{3}}$$

$$\Delta V = \frac{2T_{min}}{\sqrt{3}T_s} V_{dc} \tag{3}$$

where V_{dc} is the voltage of the DC link capacitor.

Sector 1 of the output voltage hexagon is divided into four regions composed of effective voltage vectors for the reference voltage vector V_{ref} duration, as shown in Figure 8. When the reference voltage vector is located as shown in Figure 8, the effective voltage vector and the duration time are expressed as follows:

$$V_{13}T_a + V_7T_b + V_{14}T_c = V_{ref}T_s$$
$$T_a + T_b + T_c = T_s \quad (4)$$

where T_a, T_b, and T_c are the duration time of V_{13}, V_7, and V_{14}, respectively.

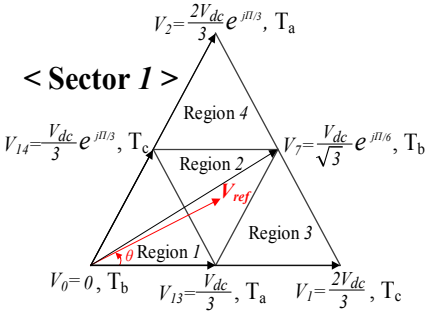

Figure 8. Sector 1 divided into four regions.

From Equation (4), the duration time of the effective voltage vectors T_a, T_b, and T_c in each region can be obtained through the equations given in Table 2. When T_a, T_b, and T_c are shorter than T_{min}, phase current cannot be obtained from the shunt resistor accurately. Therefore, it is a CUA.

Table 2. Dwell times of the voltage vector according to the regions.

Region	T_a	T_b	T_c
1	$T_s(2\sqrt{3}\frac{V_{ref}}{V_{dc}}\sin(\frac{\pi}{3}-\theta))$	$T_s(1-2\sqrt{3}\frac{V_{ref}}{V_{dc}}\sin(\frac{\pi}{3}+\theta))$	$T_s(2\sqrt{3}\frac{V_{ref}}{V_{dc}}\sin\theta)$
2	$T_s(1-2\sqrt{3}\frac{V_{ref}}{V_{dc}}\sin\theta)$	$T_s(2\sqrt{3}\frac{V_{ref}}{V_{dc}}\sin(\frac{\pi}{3}+\theta)-1)$	$T_s(1-2\sqrt{3}\frac{V_{ref}}{V_{dc}}\sin(\frac{\pi}{3}-\theta))$
3	$T_s(2-2\sqrt{3}\frac{V_{ref}}{V_{dc}}\sin(\frac{\pi}{3}+\theta))$	$T_s(2\sqrt{3}\frac{V_{ref}}{V_{dc}}\sin\theta)$	$T_s(2\sqrt{3}\frac{V_{ref}}{V_{dc}}\sin(\frac{\pi}{3}-\theta)-1)$
4	$T_s(2\sqrt{3}\frac{V_{ref}}{V_{dc}}\sin\theta-1)$	$T_s(2\sqrt{3}\frac{V_{ref}}{V_{dc}}\sin(\frac{\pi}{3}-\theta))$	$T_s(2-2\sqrt{3}\frac{V_{ref}}{V_{dc}}\sin(\frac{\pi}{3}+\theta))$

4. Conventional Method of Phase Current Reconstruction

4.1. Modified Voltage Modulation Method

The method in [7] with the alternative switching pattern is different from the classical SVPWM. The zero vector is replaced with a pair of effective voltage vectors in order to increase the duration time of the effective voltage vector, which does not ensure T_{min}. As a result, only one phase current measurable region (Area 2) can be compensated. If the reference voltage vector V_{ref} is in Area 2, as shown in Figure 9a, phase C current is unmeasurable and the zero vector [OOO] is replaced with a pair of effective voltage vectors V_{14} [OON] and V_{17} [NNO], as shown in Figure 10. Therefore, only the current of one phase can be reconstructed during one PWM period due to the variation of the switching time. However, if the reference voltage vector V_{ref} is in Area 3, as shown in Figure 9b, it needs two switching cycles. Therefore, the THD of phase current is high, because a pair of vectors, which are located at opposite positions to each other, are used to make the reference voltage.

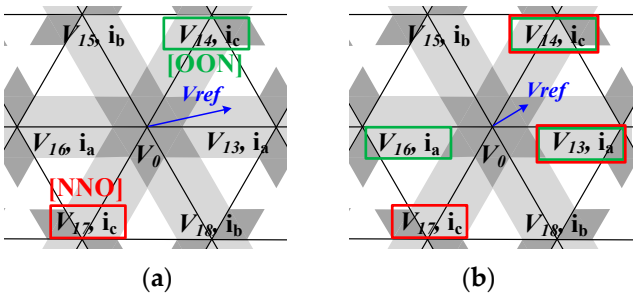

Figure 9. Duration of the reference voltage vector in CUAs. (**a**) Area 2; (**b**) Area 3.

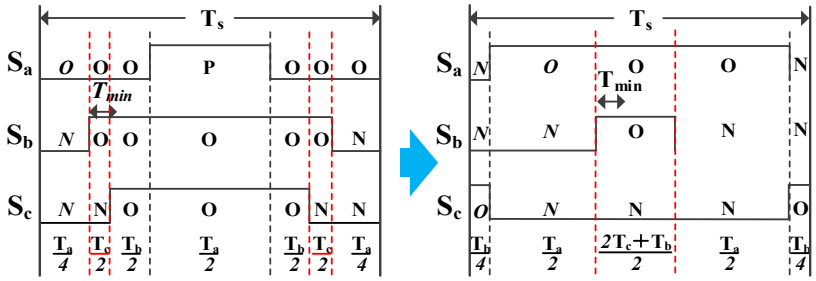

Figure 10. Switching sequences in conventional SVPWM and modified voltage modulation method. (Area 2).

4.2. Minimum Voltage Injection (MVI) Method

In this conventional method [6], the minimum voltage injection method is applied to measure the phase current, as shown in Figure 11. Figure 11a shows the reference voltage vector V_{ref} in Area 3, where two phase currents cannot be obtained. In this case, a constant voltage is added to the reference voltage vector to reconstruct the phase current. The reference voltage moved to measurable Area 1 is defined as V_m. The compensation voltage vector V_c is applied by subtracting the constant voltage which has the same magnitude as the added value to the command voltage vector. This compensation method is shown for one period of the switching pattern in Figure 11b. In this case, both "ONN" and "OON" are less than the minimum time T_{min}. So in a half period of modulation, the voltage V_m for the reconstruction is injected, and in the other half period, the compensation voltage V_c is injected to cancel the effect of the injected voltage.

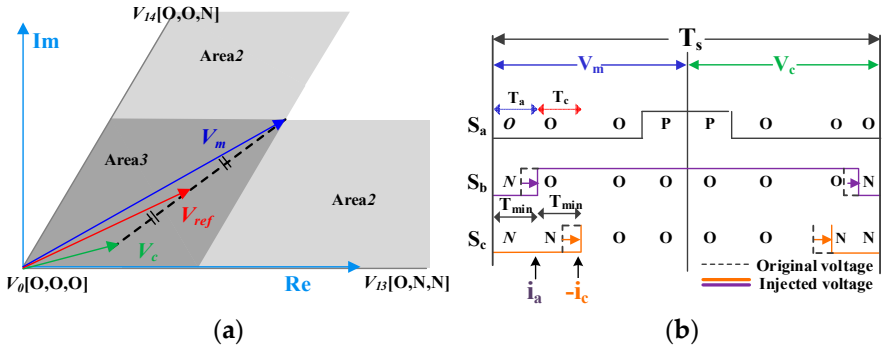

Figure 11. Minimum voltage injection method. (**a**) Voltage injection method in Area 3; (**b**) PWM switching patterns.

However, it is difficult to reconstruct the phase current using the MVI method in the high MI region shown in Figure 12. At this time, the compensation voltage V_c exceeds the linear modulation area. Therefore, it is impossible to reconstruct the phase current near the outermost edge of the hexagon.

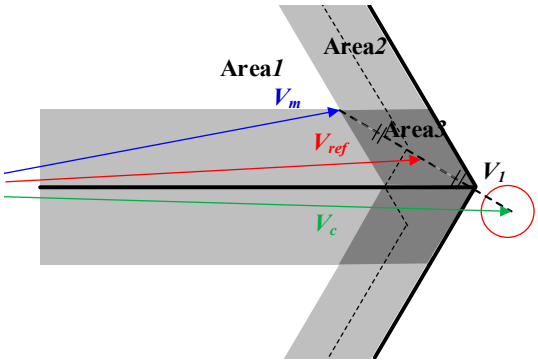

Figure 12. Voltage injection method in Area 3 beside a vertex of the hexagon.

5. Proposed Method of Phase Current Reconstruction

5.1. Based Method for Current Reconstruction in Area 2

In order to control the constant speed and constant torque of an AC motor, a current controller is essential. In general, a proportional integral (PI) controller is used on the synchronous reference frame of *d*–*q* axis [10]. Figure 13 shows the block diagram of the synchronous PI controller, and the electrical model of the motor system. Where R_a, L_a, K_p, and K_i mean the stator resistance, stator inductance, proportional gain, and integral gain, respectively. The proportional and integral gains of the PI controller are calculated using Equation (5):

$$K_p = L_a \omega_{cc} \, , \qquad K_i = R_a \omega_{cc} \tag{5}$$

where L_a is the stator inductance, R_a is the stator resistance, and ω_{cc} is the bandwidth of the PI regulator.

Then, the closed-loop transfer function $G_c(s)$ of the block diagram is given by Equation (6):

$$G_c(s) = \frac{i^e_{dq}(s)}{i^{e*}_{dq}(s)} = \frac{G_0(s)}{1 + G_0(s)} = \frac{\frac{\omega_{cc}}{s}}{1 + \frac{\omega_{cc}}{s}} = \frac{\omega_{cc}}{1 + \omega_{cc}} \tag{6}$$

According to Equations (5) and (6), the combination of the PI controller and model of the motor is equivalent to a first low-pass filter whose cutoff frequency is ω_{cc}. In this case, the real *d*–*q* axis current can be estimated using the current reference and low pass filter, as shown in Figures 13 and 14. Finally, the estimated three phase currents ($\hat{\imath}_{abc}$) can be obtained from reverse transformation of the estimated *d*–*q* axis currents ($\hat{\imath}_{dq}{}^e$). This estimated current is used to replace the unmeasurable current when the voltage command lies inside Area 2, where only one phase current is acquired. This current estimation method does not need PWM shift or voltage injection for current reconstruction.

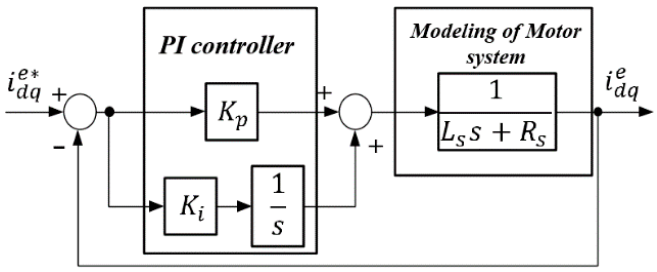

Figure 13. Block diagram of the PI controller and electrical model of the motor system.

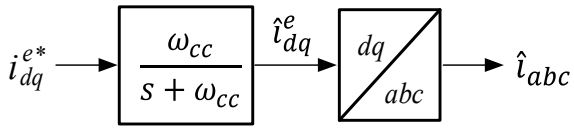

Figure 14. Block diagram of acquiring estimated current.

5.2. Proposed Method for Current Reconstruction in Area 3

In order to calculate the optimum injection voltage according to the switching sector of SVPWM, the conventional sector is classified into 36 switching sectors in this paper. These sectors can be represented by 18 straight lines, as shown in Figure 15. These straight lines can be obtained by using the two points of the hexagon. As a result, the 36 switching sectors can be defined by three straight lines. If the reference voltage vector V_{ref} is located as shown in Figure 15, straight Lines 5, 9, and 13 must be satisfied to discriminate the switching sector.

$$\text{Line 5}: V_{qs}^{s} \le -\sqrt{3}(V_{ds}^{s} - \frac{2}{3}V_{dc}),\ \ \text{Line 9}: V_{qs}^{s} \le -\sqrt{3}(V_{ds}^{s} - \frac{2}{3}V_{dc}),\ \ \text{Line 13}: V_{qs}^{s} \ge 0 \tag{7}$$

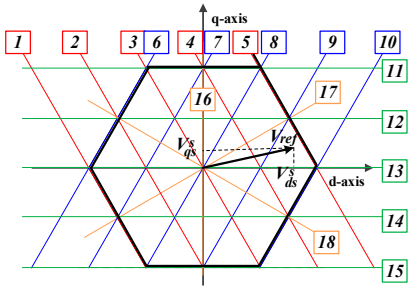

Figure 15. Lines (1–18) for the classification of 36 switching sectors.

For simple injection voltage calculation, the reference voltage vector $V_{ref}(V_{ds}^{s}, V_{qs}^{s})$ that rotates the output voltage hexagon with electrical angle θ_e, is transformed as shown in Figure 16. V_{ref} is transformed to the shifted reference voltage vector $V_{dqs}^{t}(V_{ds}^{t}, V_{qs}^{t})$ in sector 0 by Equation (8).

$$\begin{pmatrix} V_{ds}^{t} \\ V_{qs}^{t} \end{pmatrix} = \begin{pmatrix} \cos\theta_n & -\sin\theta_n \\ \sin\theta_n & \cos\theta_n \end{pmatrix} \begin{pmatrix} V_{ds}^{s} \\ V_{qs}^{s} \end{pmatrix} \tag{8}$$

where $\theta_n = n \cdot \pi/3$.

The range of the shifted sector 0 is from $-\pi/6$ to $\pi/6$. As a result, the injected voltage is only calculated in the shifted sector 0.

As shown in Figure 17a, the shifted sector is symmetrical with respect to the d-axis. Therefore, when calculating the injection voltage, only the positive part needs to be calculated. In the negative region, the negative sign can be added to the magnitude of the q component.

$V_{dqs}^{i}\left(V_{ds}^{i}, V_{qs}^{i}\right)$ are the vector components for moving V_{dqs}^{t} to the measurable region. After calculating the injection voltage, V_{dqs}^{i} is added to V_{dqs}^{t}, and reverse-transformation is executed. This voltage vector is defined as the measurement voltage vector V_{m}^{s}. V_{m}^{s} is induced during the first half period of the modulation, and the compensation voltage V_{c}^{s} is induced during the other half period. The relation between V_{ref}, V_{m}^{s}, and V_{c}^{s} is given by Equation (9).

$$V_{ref} = \frac{1}{2}(V_{m}^{s} + V_{c}^{s}) \ \rightarrow\ V_{c}^{s} = 2\left(V_{ref} - V_{m}^{s}\right) \tag{9}$$

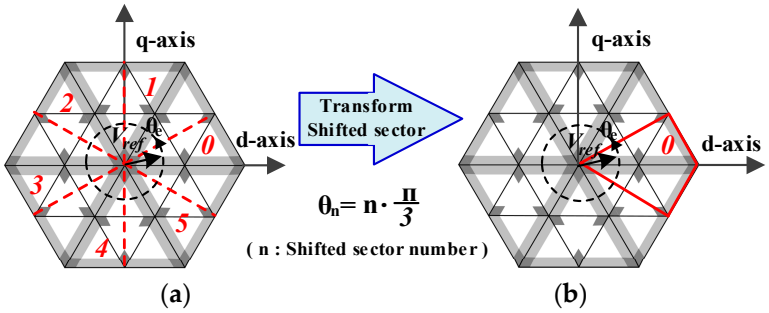

Figure 16. Transform shifted sector. (**a**) Shifted sectors (0–5); (**b**) shifted sector (0).

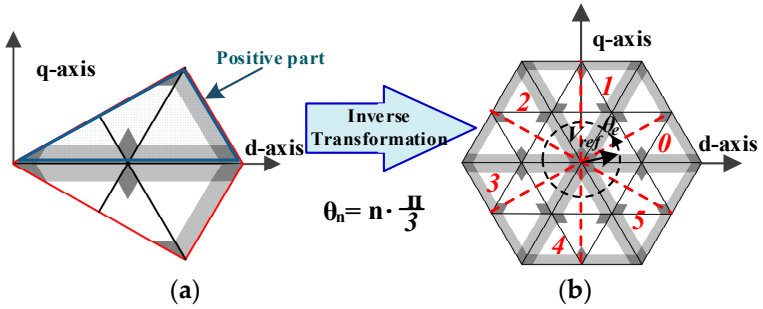

Figure 17. Inverse transformation shifted sector. (**a**) Shifted sector (0); (**b**) shifted sectors (0–5).

In order to recover the phase current by injecting the optimal voltage, the shifted sector 0 for the positive q-axis is divided into different parts, as shown in Figure 18a, according to the MI. As shown in Figure 18b, each part is more finely divided to restore the phase current by injecting the optimal voltage. Part.1 is further divided into Part.1_1 and Part.1_2, and Part.2 is divided into Part.2_1, Part.2_2, Part.2_3, and Part.2_4. Part.3 and Part.4 are also divided into two parts and four parts, respectively.

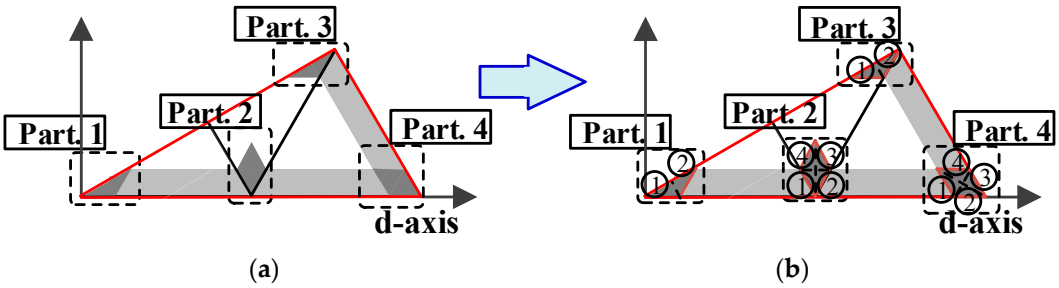

Figure 18. Detailed view of the parts of the positive shifted sector 0. (**a**) Part1–Part4; (**b**) segmentation of Parts.

When the reference voltage vector V_{ref} is located in Part.1_1, as shown in Figure 19, the optimal voltage is injected, and the measurement voltage vector V_m^s is pushed to the measurement point. At this time, the measurement point is on the boarder of Area 2. The magnitude of the injected voltage $V_{dqs}^i(V_{ds}^i, V_{qs}^i)$ can be calculated by using both the measurement point and V_{dqs}^t, as shown in Equation (10).

Part.1_1

$$V_{ds}^i = \left(2\Delta V/\sqrt{3}\right) - V_{ds}^t, \qquad V_{qs}^i = -V_{qs}^t \tag{10}$$

When the reference voltage vector is located in Part.1_2, as shown in Figure 20, the measurement voltage vector is moved to the measurement line by the optimal voltage injection. The measurement line is defined by Equation (11), with two points $(2\Delta V/\sqrt{3}, 0)$ and $(\sqrt{3}\Delta V, \Delta V)$, as the boarder of Area 2. The magnitude of the injected voltage is obtained by Equation (12), which gives the minimum

distance from the point to the measurement line through the Pythagorean theorem, as shown in Equation (13). The optimal voltage injection method is used to classify each part of Area 3 in more detail, and then bring V_m^s to the closest measurement line or measurement point for reconstructing the phase currents. At this time, the measurement line or measurement point is at the boarder of Area 1 or Area 2. Each part of Area 3 has a different type of optimal voltage injection, as shown in Equations (10) and (13)–(23), and in Figure 21.

$$y = \sqrt{3}\left(x - \sqrt{3}\Delta V\right) + \Delta V \tag{11}$$

$$d = \frac{1}{2}\left|\sqrt{3}V_{ds}^t - V_{qs}^t - 2\Delta V\right| \tag{12}$$

Part.1_2

$$\begin{aligned} V_{ds}^i &= \frac{\sqrt{3}}{2}d = \sqrt{3} \times 0.25\left(\sqrt{3}V_{ds}^t - V_{qs}^t - 2\Delta V\right), \\ V_{qs}^i &= -\frac{1}{2}d = -0.25\left(\sqrt{3}V_{ds}^t - V_{qs}^t - 2\Delta V\right) \end{aligned} \tag{13}$$

Part.2_1

$$V_{ds}^i = -\sqrt{3} \times 0.25\left(\sqrt{3}V_{ds}^t + V_{qs}^t - \frac{V_{dc}}{\sqrt{3}}\right), \quad V_{qs}^i = -\sqrt{3} \times 0.25\left(\sqrt{3}V_{ds}^t + V_{qs}^t - \frac{V_{dc}}{\sqrt{3}}\right) \tag{14}$$

Part.2_2

$$V_{ds}^i = \sqrt{3} \times 0.25\left(\sqrt{3}V_{ds}^t - V_{qs}^t - \frac{V_{dc}}{\sqrt{3}}\right), \quad V_{qs}^i = -0.25\left(\sqrt{3}V_{ds}^t - V_{qs}^t - \frac{V_{dc}}{\sqrt{3}}\right) \tag{15}$$

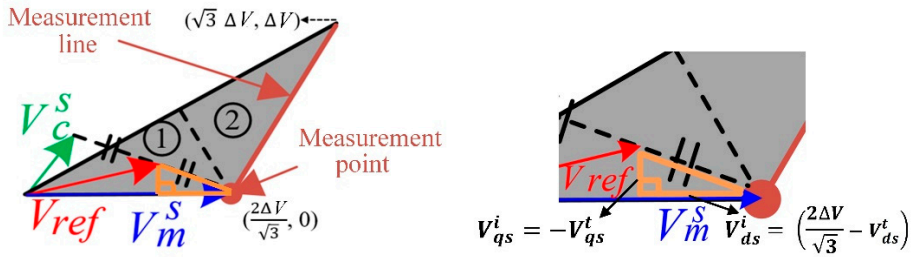

Figure 19. Optimal voltage injection method in Part.1_1. (**a**) Reference voltage vector on Part.1_1; (**b**) detailed view of the left one.

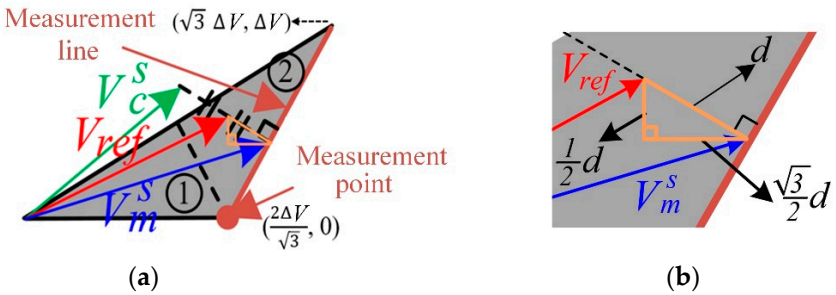

Figure 20. Optimal voltage injection method in Part.1_2. (**a**) Reference voltage vector on Part.1_2; (**b**) detailed view of the left one.

Part.2_3

$$V_{ds}^{i} = \sqrt{3} \times 0.25\left(\sqrt{3}V_{ds}^{t} + V_{qs}^{t} - \frac{V_{dc}}{\sqrt{3}} - 2\Delta V\right), \quad V_{qs}^{i} = 0.25\left(\sqrt{3}V_{ds}^{t} + V_{qs}^{t} - \frac{V_{dc}}{\sqrt{3}} - 2\Delta V\right) \tag{16}$$

Part.2_4

$$V_{ds}^{i} = -\sqrt{3} \times 0.25\left(\sqrt{3}V_{ds}^{t} - V_{qs}^{t} - \frac{V_{dc}}{\sqrt{3}} + 2\Delta V\right), \quad V_{qs}^{i} = 0.25\left(\sqrt{3}V_{ds}^{t} - V_{qs}^{t} - \frac{V_{dc}}{\sqrt{3}} + 2\Delta V\right) \tag{17}$$

Part.3_1

$$V_{ds}^{i} = 0\,, \quad V_{qs}^{i} = \left(\frac{\sqrt{3}V_{dc}}{6} - \Delta V\right) - V_{qs}^{t} \tag{18}$$

Part.3_2

$$V_{ds}^{i} = \sqrt{3}\cdot 0.25\left(\sqrt{3}V_{ds}^{t} - V_{qs}^{t} - \frac{V_{dc}}{\sqrt{3}}\right), \quad V_{qs}^{i} = -0.25\left(\sqrt{3}V_{ds}^{t} - V_{qs}^{t} - \frac{V_{dc}}{\sqrt{3}}\right) \tag{19}$$

Part.4_1

$$\begin{aligned} V_{ds}^{i} &= -\sqrt{3}\cdot 0.25\left(\sqrt{3}V_{ds}^{t} + V_{qs}^{t} - \frac{2V_{dc}}{\sqrt{3}} + 2\Delta V\right), \\ V_{qs}^{t} &= -0.25\left(\sqrt{3}V_{ds}^{t} + V_{qs}^{t} - \frac{2V_{dc}}{\sqrt{3}} + 2\Delta V\right) \end{aligned} \tag{20}$$

Part.4_2

$$V_{ds}^{i} = \left(\frac{2V_{dc}}{3} - \frac{2\Delta V}{\sqrt{3}}\right) - V_{ds}^{t}\,, \quad V_{qs}^{i} = -V_{qs}^{t} \tag{21}$$

Part.4_3

$$V_{ds}^{i} = \left(\frac{2V_{dc}}{3} - \frac{\Delta V}{\sqrt{3}}\right) - V_{ds}^{t}, \quad V_{qs}^{i} = \Delta V - V_{qs}^{t} \tag{22}$$

Part.4_4

$$V_{ds}^{i} = 0, \quad V_{qs}^{i} = \Delta V - V_{qs}^{t} \tag{23}$$

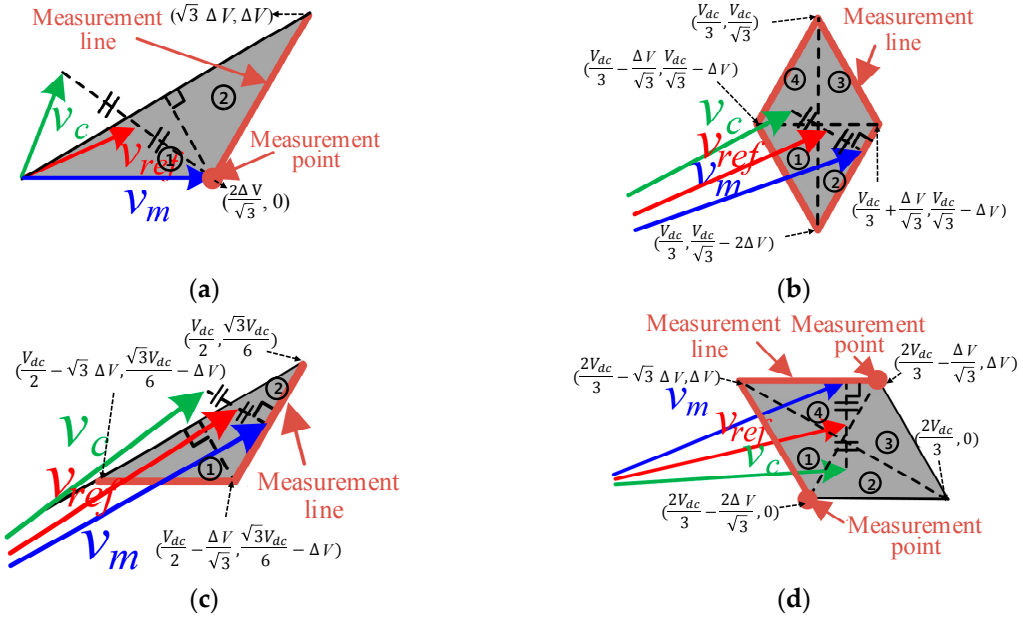

Figure 21. Optimal voltage injection method in Area 3 for each part. (**a**) Optimal voltage injection method in Part.1; (**b**) optimal voltage injection method in Part.2; (**c**) optimal voltage injection method in Part.3; (**d**) optimal voltage injection method in Part.4.

5.3. Comparison of Conventional and Proposed Method

Figure 22 shows the comparison between the proposed method and MVI method for a MI of 0.1 and 0.97. The proposed method restores the phase current by injecting a small amount of voltage when MI = 0.1 and MI = 0.97. However, the conventional method injected a large amount of voltage compared with the proposed method when MI = 0.1. In addition, the compensated voltage vector of the conventional method lies outside of the output voltage hexagon when the MI is 0.97, which makes the reconstruction of the phase current impossible.

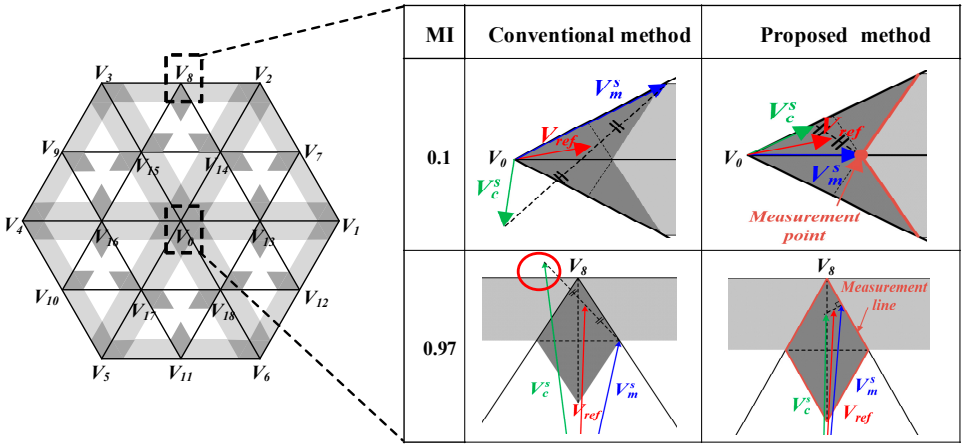

Figure 22. Comparison of conventional method and proposed method at MI = 0.1 and MI = 0.97.

As shown in Table 3, when the proposed method is applied, it can be seen that the area of the non-measurable region in the output voltage hexagon is reduced by about 93.7 % in comparison with the case in the MVI method.

Table 3. Unmeasurable area comparison.

3-Level NPCI One Shunt Unmeasurable Area	Conventional Method	Proposed Method
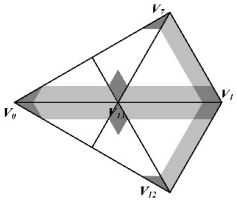	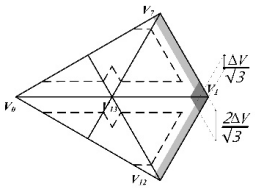	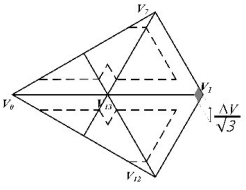
Unmeasurable area of shifted sector 0		
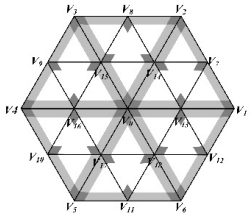	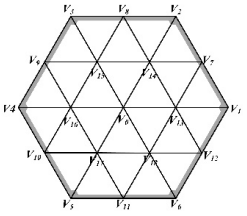	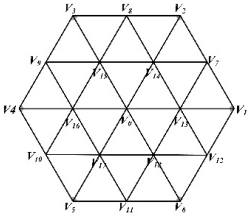
Unmeasurable area of hexagon		

6. Experimental Results

Figure 23 describes the system configuration of the experimental setup for the verification of the proposed current reconstruction method. The system was composed of the three-level NPC inverter, including the shunt resistor, connected to the neutral point, the control system based on the digital signal processor (DSP, TMS320C28346), and the resistive-inductive load. The upper and lower DC capacitors were connected with the 30 V power source.

A resistor of 10 Ω and inductor of 5 mH were used as the load. The resistance of the shunt resistor was 0.2 Ω and its power capacity was 3 W. In addition, the minimum time T_{min} needed to acquire the precise phase current from the shunt resistor was set to be 4.5 μs. The reconstructed current from the shunt resistor using the proposed algorithm was compared with an actual current measured using two current sensors in order to verify its precision.

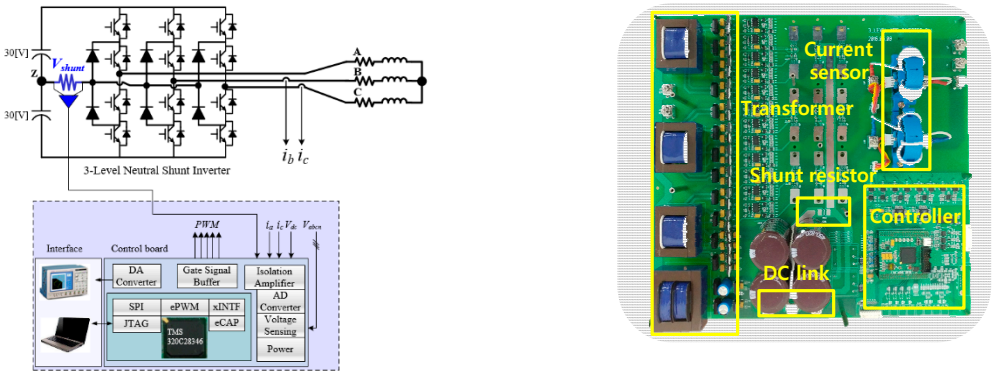

Figure 23. Configuration of hardware system and control board.

In the experiment, the inverter system was operated by the V/F open-loop control algorithm. The system was controlled with a fixed operating frequency of 12 Hz and variable output voltage to change the MI. The experimental results were classified in 6 cases to compare with the conventional MVI method. Figure 24a,b shows the experimental results with the condition of MI = 0.1 (V_{ref} = 3.56 V). In this case, the inverter was operated in Area 3 where the two currents cannot be measured from the shunt resistor. As presented in Figure 24b, the injected d–q voltage for the current reconstruction is smaller than the voltage in Figure 24a. The experimental results of Figure 24c,d was measured when the inverter was operated in Area 1 and 2 with MI of 0.4 (V_{ref} = 13.86 V). In Area 1, it is possible to obtain the two phase currents from the shunt resistor, and only one current can be acquired in Area 2. As shown in Figure 24c, the conventional method injects the q-axis voltage to reconstruct the phase current. In contrast, the proposed method can reconstruct the phase current without the voltage injection, as presented in Figure 24d, because the phase current is reconstructed using the estimated current. In Figure 24e,f, V_{ref} is passed through Area 1 and 3 when the MI is 0.6 (V_{ref} = 20.78 V). As shown in Figure 24f, a smaller voltage is injected to reconstruct the phase current in the proposed method in comparison with the conventional method. The waveforms presented in Figure 25e,f was measured when the MI was 0.97 (V_{ref} = 33.6 V). In this case, the trajectory of the voltage reference is near the inscribed circle of the space vector hexagon. In the case of the conventional method, the phase current cannot be reconstructed even if the voltage injection method is used, because the compensated voltage reference exceeds the hexagon. On the other hand, the proposed method can reconstruct the phase current, as presented in Figure 25f, because the voltage reference can be compensated on the boundary of the hexagon.

The accuracy of the phase currents reconstructed using the conventional and proposed methods were calculated to show the superiority of the proposed algorithm. The equation for the accuracy of the phase current is expressed in Equation (24).

$$Accurcy\ (\%) = \left(1 - \frac{Variance\ of\ [i_{sensor} - i_{reconstructed}]}{RMS\ of\ i_{sensor}}\right) \times 100 \tag{24}$$

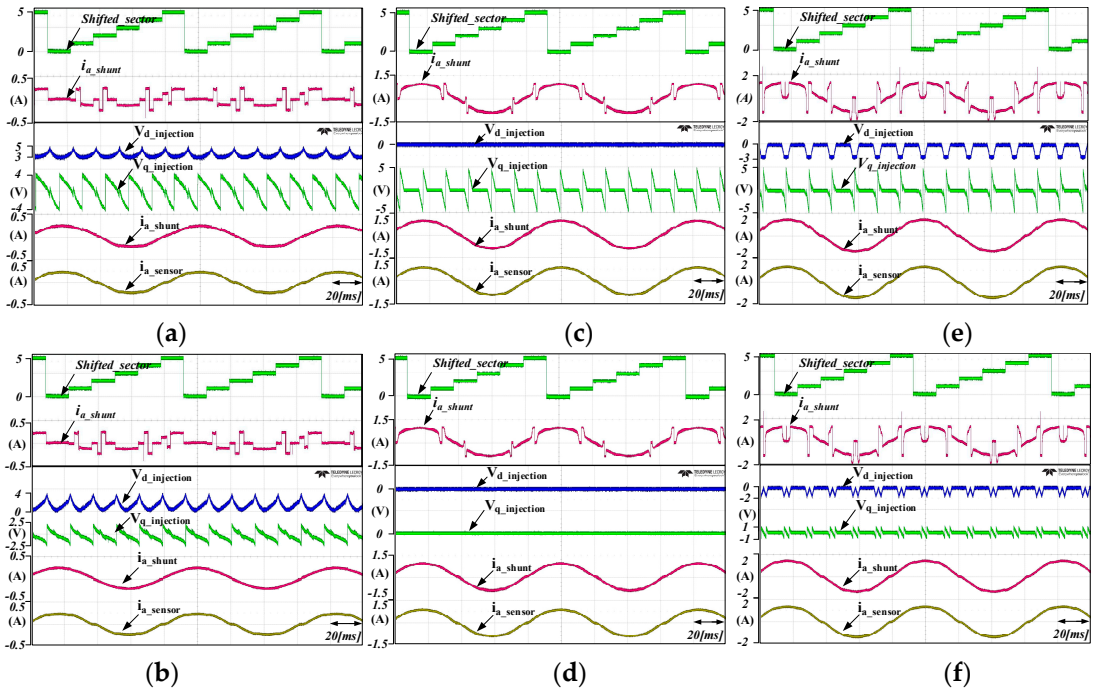

Figure 24. Comparison of the conventional and proposed methods at MI = 0.1, 0.4, and 0.6. (**a**) Conventiona method at MI = 0.1; (**b**) proposed method at MI = 0.1; (**c**) conventional method at MI = 0.4; (**d**) proposed method at MI = 0.4; (**e**) conventional method at MI = 0.6; (**f**) proposed method at MI = 0.6.

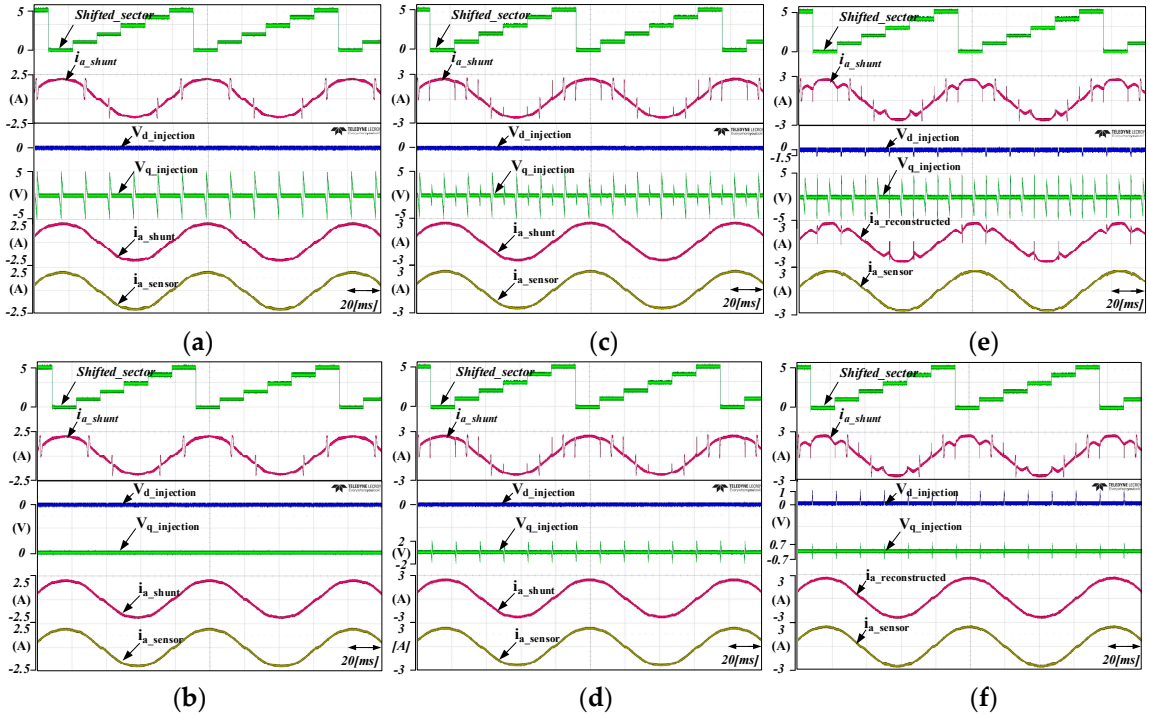

Figure 25. Comparison of the conventional and proposed methods at MI = 0.8, 0.9, and 0.97. (**a**) Conventional method at MI = 0.8; (**b**) proposed method at MI = 0.8; (**c**) conventional method at MI = 0.9; (**d**) proposed method at MI = 0.9; (**e**) conventional method at MI = 0.97; (**f**) proposed method at MI = 0.97.

As the difference between the current measured by the sensor and the reconstructed current is increased, the variance of the calculated results increases. This means the accuracy of the reconstruction is low. The difference in accuracy between the conventional method and the proposed method is

compared according to the MI, and shown in Figure 26a. The accuracy of the proposed method is higher than the conventional method in the whole range of the MI.

The comparison results for the THD of the phase current between the conventional method and the proposed method are presented in Figure 26b.

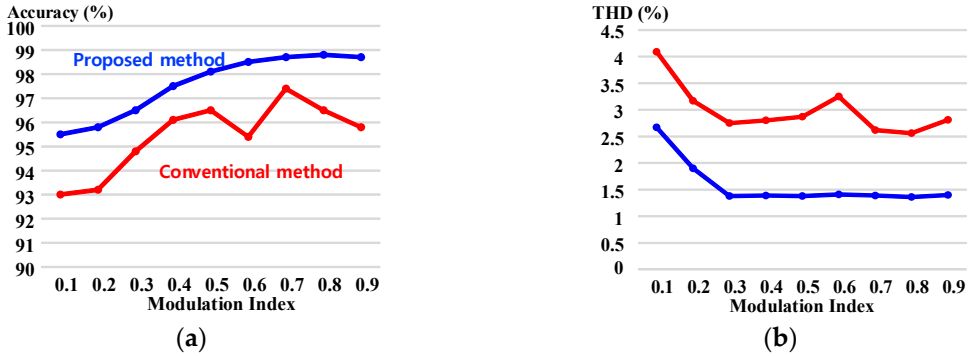

Figure 26. Comparison of the conventional and proposed methods according to the variation in the MI. (**a**) Phase current Accuracy; (**b**) total harmonic distortion (THD) of phase currents.

The THD result for the proposed method is lower than the result for the conventional method in the whole range of the MI, because the THD of the phase current is proportional to the injected voltage. On average the THD of the proposed method is improved by 44.5 % compared with that of the conventional method.

7. Conclusions

This paper proposed a phase current reconstruction method using a neutral shunt resistor, which lowers both the cost and volume of a three-level inverter system.

First, the paper proposes the method for dividing the switching sectors, the rotated sectors, and the region. Each region is separated by the equation of a straight line.

In addition, in Area 2 where there is only one measurable phase current, the remaining phase current is reconstructed by the estimation method. The electrical model of the motor and PI current controller are used to estimate the current.

Finally, the optimal voltage injection method is used in Area 3, where no current is acquired through the shunt resistor (CUAs). Area 3 is divided and defined as parts in more detail. When the reference is located on Area 3 of the hexagon, the phase currents are reconstructed by moving the reference vector to the border of Area 1 or Area 2.

The proposed method utilized a small magnitude injection voltage compared to the conventional method, and hence results in better performance in terms of THD and accuracy of the estimated currents. The validity of the proposed algorithm is proven by the experiments.

Author Contributions: Y.S. contributed to the research activity and to manuscript writing. J.K. provided technical feedback and did supervision of the overall work.

Funding: This research received no external funding.

Acknowledgments: This research was supported by the Basic Science Research Program through the National Research Foundation of Korea (NRF) funded by the Ministry of Education (NRF-2018R1D1A1B07048954).

Conflicts of Interest: The authors declare no conflict of interest.

References

1. De, S.; Banerjee, D.; Gopakumar, K.; Ramchand, R.; Patel, C. Multilevel inverters for low-power application. *IET Power Electron.* **2010**, *4*, 382–392. [CrossRef]
2. Lipo, T.A.; Manjrekar, M.D. Hybrid Topology for Multilevel Power Conversion. U.S. Patent 06,005,788, 21 December 1999.
3. Lai, R.; Wang, F.; Burgos, R.; Pei, Y.; Boroyevich, D.; Wang, B.; Lipo, T.A.; Immanuel, V.D.; Karimi, K.J. A systematic topology evaluation methodology for high-density three-phase PWM AC-AC converters. *IEEE Trans. Power Electron.* **2008**, *23*, 2665–2680.
4. Heldwein, M.L.; Kolar, J.W. Impact of EMC filters on the power density of modern three-phase PWM converters. *IEEE Trans. Power Electron.* **2009**, *24*, 1577–1588. [CrossRef]
5. Jarzebowicz, L. Error Analysis of Calculating Average d-q Current Components using Regular Sampling and Park Transformation in FOC Drives. In Proceedings of the 2014 International Conference and Exposition on Electrical and Power Engineering (EPE 2014), Iasi, Romania, 16–18 October 2014; pp. 901–905.
6. Shin, H.; Ha, J.I. Phase Current Reconstructions from DC-Link Currents in Three-Phase Three-Level PWM Inverters. *IEEE Trans. Power Electron.* **2014**, *29*, 582–593. [CrossRef]
7. Li, X.; Dusmez, S.; Akin, B.; Rajashekara, K. A New SVPWM for the Phase Current Reconstruction of Three-Phase Three-level T-type Converters. *IEEE Trans. Power Electron.* **2015**, *62*, 2627–2637.
8. Blaabjerg, F.; Pedersen, J.K. An ideal PWM-VSI inverter using only one current sensor in the DC-link. In Proceedings of the 1994 Fifth International Conference on Power Electronics and Variable-Speed Drives, London, UK, 26–28 October 1994; pp. 458–464.
9. Lee, W.C.; Hyun, D.S.; Lee, T.K. A Novel Control Method for Three-Phase PWM Rectifiers Using a Single Current Sensor. *IEEE Trans. Power Electron.* **2000**, *15*, 861–870.
10. Yeom, H.B.; Ku, H.K.; Kim, J.M. Current reconstruction method for PMSM drive system with a DC link shunt resistor. In Proceedings of the 2016 IEEE Energy Conversion Congress and Exposition (ECCE), Milwaukee, WI, USA, 18–22 September 2016; pp. 18–22.
11. Ha, J.I. Voltage Injection Method for Three-Phase Current Reconstruction in PWM Inverters Using a Single Sensor. *IEEE Trans. Power Electron.* **2009**, *24*, 767–775.
12. You, J.J.; Jung, J.H.; Park, C.H.; Kim, J.M. Phase current reconstruction of three-level Neutral-Point-Clamped (NPC) inverter with a neutral shunt resistor. In Proceedings of the 2017 IEEE Applied Power Electronics Conference and Exposition (APEC), Tampa, FL, USA, 26–30 March 2017; pp. 2598–2604.
13. Gu, Y.; Ni, F.; Yang, D.; Liu, H. Switching-State Phase Shift Method for Three-Phase-Current Reconstruction with a Single DC-Link Current Sensor. *IEEE Trans. Ind. Electron.* **2011**, *58*, 5186–5194.
14. Lin, Y.K.; Lai, Y.S. PWM Technique to Extend Current Reconstruction Range and Reduce Common-Mode Voltage for Three-Phase Inverter using DC-link Current Sensor Only. In Proceedings of the 2011 IEEE Energy Conversion Congress and Exposition, 12–16 September 2011; pp. 1978–1985.
15. Lai, Y.S.; Lin, Y.K.; Chen, C.W. New Hybrid Pulse width Modulation Technique to Reduce Current Distortion and Extend Current Reconstruction Range for a Three-Phase Inverter Using Only DC-link Sensor. *IEEE Trans. Power Electron.* **2013**, *28*, 1331–1337. [CrossRef]
16. Lu, H.; Cheng, X.; Qu, W.; Sheng, S.; Li, Y.; Wang, Z. A Three-Phase Current Reconstruction Technique Using Single DC Current Sensor Based on TSPWM. *IEEE Trans. Power Electron.* **2014**, *29*, 1542–1550.
17. Ying, L.; Ertugrul, N. An Observer-Based Three-Phase Current Reconstruction using DC Link Measurement in PMAC Motors. In Proceedings of the 2006 CES/IEEE 5th International Power Electronics and Motion Control Conference, Shanghai, China, 14–16 August 2006; pp. 1–5.
18. Saritha, B.; Janakiraman, P.A. Sinusoidal Three-Phase Current Reconstruction and Control Using a DC-Link Current Sensor and a Curve-Fitting Observer. *IEEE Trans. Ind. Electron.* **2007**, *54*, 2657–2664. [CrossRef]
19. Kim, K.; Yeom, H.; Ku, H.; Kim, J. Current reconstruction method with single DC-link. In Proceedings of the 2014 IEEE Energy Conversion Congress and Exposition, 14–18 September 2014; pp. 250–256.
20. Tomigashi, Y.; Hida, H.; Ueyama, K. Voltage vector correction based on a novel coordinate transformation for motor current detection using a single shunt resistor. In Proceedings of the 2009 13th European Conference on Power Electronics and Applications, 8–10 September 2009; pp. 1–8.

21. Kim, H.; Jahns, T.M. Integration of the Measurement Vector insertion Method (MVIM) with Discontinuous PWM for Enhanced Single Current Sensor Operation. In Proceedings of the 2006 IEEE Industry Applications Conference Forty-First IAS Annual Meeting, 8–12 October 2006; Volume 5, pp. 2459–2465.
22. Carpaneto, M.; Marchesoni, M.; Parodi, G. A Sensorless PMSM Drive Operating in the Field Weakening Region Using Only One Current Sensor. In Proceedings of the 2010 IEEE International Symposium on Industrial Electronics (ISIE), 4–7 July 2010; pp. 1199–1204.
23. Bing, Z.; Du, X.; Sun, J. Control of three-phase PWM rectifiers using a single DC current sensor. *IEEE Trans. Power Electron.* **2011**, *26*, 1800–1808. [CrossRef]
24. Sun, K.; Wei, Q.; Huang, L.; Matsuse, K. An overmodulation method for PWM-inverter-fed IPMSM drive with single current sensor. *IEEE Trans. Ind. Electron.* **2010**, *57*, 3395–3404. [CrossRef]